

Polarization-entangled photon pairs from a periodically poled crystalline waveguide

Zachary H. Levine,¹ Jingyun Fan,^{1,2} Jun Chen,^{1,2}
and Alan L. Migdall^{1,2}

¹*Optical Technology Division, National Institute of Standards and Technology, Gaithersburg, Maryland 20899-8441, USA*

²*Joint Quantum Institute, University of Maryland, College Park, Maryland 20742, USA*

*levine@nist.gov

Abstract: A proposal is made for the generation of polarization-entangled photon pairs from a periodically poled crystal allowing for high collection efficiency, high entanglement, and stable operation. The theory is formulated for colinear propagation for application to waveguides. The key feature of the theory is the use of type II phase matching using both the +1 and -1 diffraction orders of the poling structure. Although these conditions are fairly restrictive in terms of operating parameters, practical operating conditions can be found. For example, we find that a HeNe pump laser may be used for a periodically poled rubidium-doped potassium titanyl phosphate (Rb:KTP) waveguide to yield single mode polarization-entangled pairs. Fidelities of 0.98 are possible under practical conditions.

© 2011 Optical Society of America

OCIS codes: (190.4975) Parametric processes; (270.1670) Coherent optical effects; (130.2790) Guided waves.

References and links

1. J.-W. Pan, D. Bouwmeester, M. Daniell, H. Weinfurter, and A. Zeilinger, "Experimental test of quantum nonlocality in three-photon greenberger-horne-zeilinger entanglement," *Nature* **403**, 515–519 (2000).
2. D. Bouwmeester, J.-W. Pan, K. Mattle, M. Eibl, H. Weinfurter, and A. Zeilinger, "Experimental quantum teleportation," *Nature* **390**, 575–579 (1997).
3. M. P. Peloso, I. Gerhardt, C. Ho, A. Lamas-Linares, and C. Kurtsiefer, "Daylight operation of a free space, entanglement-based quantum key distribution system," *N. J. Phys.* **11**, 045007 (2009).
4. Z. Y. Ou and L. Mandel, "Violation of bell's inequality and classical probability in a two-photon correlation experiment," *Phys. Rev. Lett.* **61**, 50–53 (1988).
5. P. G. Kwiat, K. Mattle, H. Weinfurter, and A. Zeilinger, "New high-intensity source of polarization-entangled photon pairs," *Phys. Rev. Lett.* **75**, 4337–4341 (1995).
6. P. G. Kwiat, E. Waks, A. G. White, I. Appelbaum, and P. H. Eberhard, "Ultrabright source of polarization-entangled photons," *Phys. Rev. A* **60**, 773–776 (1999).
7. A. Rossi, G. Vallone, A. Chiuri, F. D. Martini, and P. Mataloni, "Multipath entanglement of two photons," *Phys. Rev. Lett.* **102**, 153902 (2009).
8. J. T. Barreiro, N. K. Langford, N. A. Peters, and P. G. Kwiat, "Generation of hyperentangled photon pairs," *Phys. Rev. Lett.* **95**, 260501 (2005).
9. T. Kim, M. Fiorentino, and F. N. C. Wong, "Phase-stable source of polarization-entangled photons using a polarization sagnac interferometer," *Phys. Rev. A* **73**, 012316 (2006).
10. R. W. Risk, "Fabrication and characterization of planar ion-exchanged ktiopo₄ waveguides for frequency doubling," *Appl. Phys. Lett.* **58**, 19–21 (1991).
11. P. Baldi, P. Aschieri, S. Noh, M. D. Micheli, D. B. Ostrowsky, D. Delacourt, and M. Papuchon, "Modeling and experimental observation of parametric fluorescence in periodically poled lithium niobate waveguides," *IEEE J. Quantum Electron.* **31**, 997–1008 (1995).

12. M. M. Fejer, G. A. Magel, D. H. Jundt, and R. L. Byer, "Quasi-phase-matched second harmonic generation: Tuning and tolerances," *IEEE J. Quantum Electron.* **28**, 2631–2654 (1992).
13. Technically, the c_m are frequency-dependent, however, because their frequency dependence is scaled to the band gap of (3.6 eV for KTP) whereas that of $\beta(\omega_s, \omega_i)$ is scaled to the width of phase matching. For practical crystal lengths $L \gtrsim 10$ mm, this width is 1 meV or less, so the c_m may be treated as constants.
14. J. Chen, A. J. Pearlmund, A. Ling, J. Fan, and A. Migdall, "A versatile waveguide source of photon pairs for chip-scale quantum information processing," *Opt. Express* **17**, 6727–6740 (2009).
15. R. Jozsa, "Fidelity for mixed quantum states," *J. Mod. Opt.* **41**, 2315–2323 (1994).
16. C. E. Kuklewicz, M. Fiorentino, G. Messin, F. N. C. Wong, and J. H. Shapiro, "High-flux source of polarization entangled photons from a periodically poled ktiopo₄ parametric down-converter," *Phys. Rev. A* **69**, 013807 (2004).
17. M. Fiorentino, S. M. Spillane, R. G. Beausoleil, T. D. Roberts, P. Battle, and M. W. Munro, "Spontaneous parametric down-conversion in periodically poled ktp waveguides and bulk crystals," *Opt. Express* **15**, 7479–7488 (2007).
18. A. Fedrizzi, T. Herbst, A. Poppe, T. Jennewein, and A. Zeilinger, "A wavelength-tunable fiber-coupled source of narrowband entangled photons," *Opt. Express* **15**, 15377–15386 (2007).
19. T. Zhong, F. N. C. Wong, T. D. Roberts, and P. Battle, "High performance photon-pair source based on a fiber-coupled periodically poled ktiopo₄ waveguide," *Opt. Express* **17**, 12019–12029 (2009).
20. M. H. Rubin, D. N. Klyshko, Y. H. Shih, and A. V. Sergienko, "Theory of two-photon entanglement in type-II parametric down-conversion," *Phys. Rev. A* **50**, 5122–5133 (1994).
21. M. Katz, D. Eger, H. Kim, L. Jankovic, G. Stegeman, S. Carrasco, and L. Torner, "Second harmonic generation tuning curves in quasiphase-matched potassium titanyl phosphate with narrow, high-intensity beams," *J. Appl. Phys.* **93**, 8852–8861 (2003).
22. G. K. Samanta, S. C. Mathew, C. Canalias, V. Pasiskevicius, F. Laurell, and M. Ebrahim-Zadeh, "High-power, continuous-wave, second-harmonic generation at 532 nm in periodically poled ktiopo₄," *Opt. Lett.* **33**, 2955–2957 (2008).
23. F. Torabi-Goudarzi and E. Riis, "Efficient cw high-power frequency doubling in periodically poled ktp," *Opt. Commun.* **227**, 389–403 (2003).
24. F. König and F. N. C. Wong, "Extended phase matching of second-harmonic generation in periodically poled ktiopo₄ with zero group-velocity mismatch," *Appl. Phys. Lett.* **84**, 1644–1646 (2004).
25. K. Frakin, A. Arie, A. Skliar, and G. Rosenman, "Tunable midinfrared source by difference frequency generation in bulk periodically poled ktiopo₄," *Appl. Phys. Lett.* **74**, 914–916 (1999).
26. L. K. Cheng, L. T. Cheng, J. Galperin, P. A. M. Hotsenpiller, and J. D. Bierlein, "Crystal-growth and characterization of ktiopo₄ isomorphs from the self-fluxes," *J. Cryst. Growth* **137**, 107 (1994).
27. <http://www.comsol.com>. Mention of commercial products is for information only; it does not imply recommendation or endorsement by NIST.
28. J. D. Bierlein, A. Ferretti, L. H. Brixner, and W. Y. Hsu, "Fabrication and characterization of optical waveguides in ktiopo₄," *Appl. Phys. Lett.* **50**, 1216 (1987).
29. S. Emanueli and A. Arie, "Temperature-dependent dispersion equations for ktiopo₄ and ktioaso₄," *Appl. Opt.* **42**, 6661 (2003).
30. T. Mikami, T. Okamoto, and K. Kato, "Sellmeier and thermo-optic dispersion formulas for rbtio₄," *Appl. Opt.* **42**, 6661 (2003).
31. S. L. Braunstein, A. Mann, and M. Revzen, "Maximal violation of bell inequalities for mixed states," *Phys. Ref. Lett.* **68**, 1992 (1992).
32. P. G. Kwiat, "Hyper-entangled states," *J. Mod. Opt.* **44**, 2173 (1997).
33. R. C. Miller, "Optical second harmonic generation in piezoelectric crystals," *Appl. Phys. Lett.* **5**, 17–19 (1964).

1. Introduction

Photonic entanglement is essential to the study of fundamental physics and quantum information science. Polarization is frequently used as the entanglement degree of freedom although other variables such as momentum, orbit-angular-momentum, time and energy are also choices. Many pioneering experiments such as a non-locality test [1] and quantum teleportation [2] were explored using polarization-entangled photons. Recently field tests for quantum-key-distribution with polarization-entangled photon pairs have begun [3]. These applications demand the development of a simple, high quality source of polarization-entangled photon pairs. We propose and model a new scheme that offers efficient collection, high entanglement fidelity, and stable, convenient operation.

While the principle has been around for a long time [4], the most common sources of

polarization-entangled photons still create pairs via spontaneous parametric down conversion (SPDC) in nonlinear crystals, and advances continue to be made. The basic design has been to effectively create two pair sources with orthogonal polarization and place them so that one cannot determine which source generated the pair other than through the emitted polarization thus yielding entangled pairs. The first such source used type-II phase-matched SPDC in which the down-converted photons were emitted into two non-concentric cones, one with ordinary polarization and the other with extraordinary polarization. These two cones intersect along two lines with polarization-entangled photon pairs collected only along those two special angular directions [5]. In 1999, Kwiat and his colleagues demonstrated a new source scheme using type-I SPDC where an extraordinary polarized pump produces two photons that have matching ordinary polarizations [6]. They stacked together two such identical thin nonlinear crystals but rotated one crystal 90° about the pump direction. The pump laser beam is linearly polarized at 45° with respect to both crystals' extraordinary axes. Half of the pump beam light drives a type-I parametric down-conversion process in one crystal; the other half drives an identical type-I parametric down-conversion process in the second crystal, but with polarizations of pump and two daughter fields orthogonal to the corresponding fields in the first crystal. The entire emission cones of the two type-I parametric processes nearly perfectly overlap each other. Polarization-entangled photon pairs can be selected from any azimuthal angle around the axis of the cone. This bright source allows many interesting applications such as high-dimensional entanglement [7] and hyper-entanglement [8]. A new polarization-entangled-pair source development was contributed recently by Kim, Fiorentino, and Wong [9]. They placed a periodically poled Potassium Titanyl Phosphate (PPKTP) crystal in a Sagnac interferometer. Pump beams entering each end of the crystal coherently drove two identical type-II SPDC processes. The Sagnac arrangement combines the output of the two SPDC processes so that the creation direction cannot be determined, the yielding entangled photon pairs. The advantage of this source is that all beams propagate coaxially, greatly easing the optical alignment including the collection of entangled photons which has been cumbersome in previous sources.

In this paper, we propose a new source scheme for polarization-entangled photon pairs, one which builds on the two-source theme of Kwiat and co-workers [5, 6] and Kim *et al.* [9] by effectively creating two sources within a single crystal and using only a single pass of the pump laser beam through that crystal. With a proper choice of poling period and a simple compensation of the temporal walk-off, an entanglement fidelity near unity can be achieved.

Our scheme, shown in Fig. 1, employs a periodically poled waveguide in which two different type-II SPDC processes occur. Each of the processes are quasi-phase matched type II SPDC but the poling contributes a wave vector of opposite sign for the two different processes, as illustrated in Fig. 1(b). Typical optics for a two-photon coincidence experiment are shown in Fig. 1(c). This arrangement takes advantage of the high two-photon brightness made possible by quasi-phase matching and periodic poling and a waveguide geometry is used to limit the pair production to a single spatial mode. The waveguide is formed by the diffusion of Rb [10] into KTP which displaces some of the K ions in the lattice, forming an alloy of Rubidium Titanyl Phosphate (RTP) and KTP varying from pure RTP at the surface to pure KTP at a depth of tens of micrometers. (We denote this system as an Rb:KTP waveguide.) The complexity of the alignment is much reduced compared to previous sources, leading to superior stability and high fidelity.

2. Polarization-entangled two-photon state in a crystalline waveguide

Quasi-phase matching has been extensively applied in SPDC to create photon pairs at chosen wavelengths [11]. In quasi-phase matching, the domain of the crystal of length $L = 2\ell$ is reversed in a pattern with period Λ , called the poling period, so that the usual wave vectors of

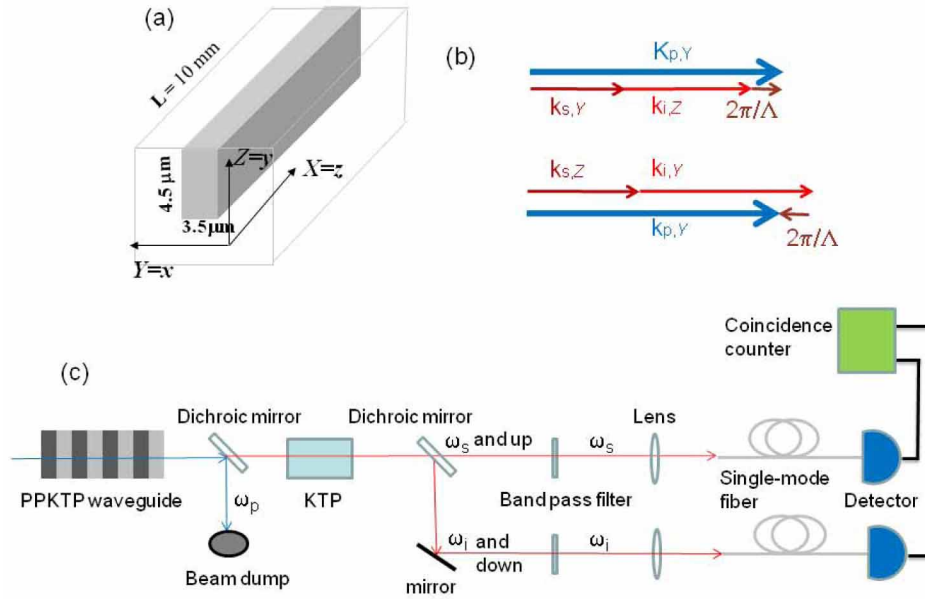


Fig. 1. Optical system for the generation of polarization-entangled photons. (a) A waveguide in KTP, showing the crystal axes X , Y , and Z . The crystal axes are aligned along spatial z , x , and y , respectively. The region of high R_b is shown. (b) An illustration of two different ways to achieve type-II phase matching. (c) The optical system for a two-photon interference experiment. The first dichroic mirror prevents parametric down conversion in the temporal KTP compensator. The beams enter a bulk KTP crystal whose length is 0.4844 of the length of the waveguide and whose orientation is rotated 90° about the optic axis with respect to the KTP waveguide, i.e., matching the spatial axes (x, y, z) to the crystal axes $(-Z, Y, X)$. The beams are then separated with a dichroic mirror and filtered to remove down converted photons from higher harmonics of the poling period. The mirror on the idler branch may have a polarization dependent reflectivity which may enhance the fidelity as discussed in the text. The beams are coupled into unpolarized single mode optical fibers.

phase matching are supplemented by wave vectors corresponding to $2\pi/\Lambda$ times an integer m [12]. If the pattern is chosen to correspond to a square wave with a 50 % duty cycle, then the additional spatial frequencies are $2m\pi/\Lambda$ but include only the integer pairs $m = \pm 1, \pm 3$. To avoid an edge effect, L should be in an integral multiple of Λ , although $L \gg \Lambda$ is a sufficient condition. (Hereafter we will not distinguish between phase matching and quasi-phase matching.)

Spontaneous parametric down conversion in a waveguide which supports only a single mode for the daughter photons yields a two-photon state which may be written as

$$|\bar{2}\rangle = 4 \int d\omega_s d\omega_i d\vec{r}_s d\vec{r}_i \beta(\omega_s, \omega_i) U_Y(\vec{r}_s, \omega_s) U_Z(\vec{r}_i, \omega_i) a_Y^\dagger(\vec{r}_s, \omega_s) a_Z^\dagger(\vec{r}_i, \omega_i) |0\rangle, \quad (1)$$

where the spatial integral is taken over the waveguide, the angular frequencies are each integrated from $-\infty$ to ∞ , $\beta(\omega_s, \omega_i)$ is a two-photon joint spectral amplitude, where ω_s and ω_i are the frequencies of the signal and idler fields, $U_j(\vec{r}, \omega)$ is the spatial mode of the waveguide, for polarizations along crystal axes $j = Y, Z$, $a_j^\dagger(\vec{r}, \omega)$ is the creation operator for a photon at a point \vec{r} with angular frequency ω and polarization j , and $|0\rangle$ is the photonic ground state. We use the convention that a bar over a state is unnormalized. We consider the case in which the confined modes at both the signal and idler frequencies are unique (i.e., single mode) for each

of the two polarizations. The effect of the slightly different spatial modes for each polarization proves to be modest, so we defer its treatment to Appendix A. Neglecting the effect of spatial modes, Eq. (1) reduces to

$$|\bar{2}\rangle = 4 \int d\omega_s d\omega_i \beta(\omega_s, \omega_i) a_Y^\dagger(\omega_s) a_Z^\dagger(\omega_i) |0\rangle, \quad (2)$$

where the creation operators create photons in a mode with a fixed spatial dependence.

The pump photon with angular frequency ω_p turns into a signal and idler photon pair. Energy is conserved, so $\omega_p = \omega_s + \omega_i$. If we consider parametric down conversion in a straight crystalline waveguide or a bulk crystal of length $L = 2\ell$, the joint spectral amplitude is given by

$$\beta(\omega_s, \omega_i) = \alpha(\omega_s + \omega_i) \sum_{m=-\infty}^{\infty} c_m \text{sinc}[\Delta k_m(\omega_s, \omega_i)\ell]. \quad (3)$$

Here, $\alpha(\omega_p)$ is the pump spectrum, $\text{sinc}[\Delta k_m(\omega_s, \omega_i)\ell]$ is a phase matching function, and the c_m are taken to be constants [13].

A typical choice for the pump spectrum in Eq. (3) is the Gaussian

$$\alpha(\omega_p) = \frac{1}{(2\pi)^{1/4} \sigma_p^{1/2}} \exp\left(-\frac{(\omega_p - \omega_p^{(1)})^2}{4\sigma_p^2}\right), \quad (4)$$

where $\omega_p^{(1)}$ is the central pump angular frequency and σ_p is the width. We have chosen the constants in Eq. (4) so that for the CW case

$$\lim_{\sigma_p \rightarrow 0} [\alpha(\omega_p)]^2 = \delta(\omega_p - \omega_p^{(1)}). \quad (5)$$

We only consider the CW case in this paper.

A key feature here is that we assume $c_1 \approx c_{-1}$ in Eq. (3) and that all the other c_m may be neglected. (The first assumption is justified in Appendix B. The terms c_m with $|m| > 1$ may be neglected because the effective nonlinear coefficient $d_{\text{eff}} = 2d_{\text{bulk}}/(|m|\pi)$, so the $m = \pm 1$ terms are the largest; moreover, the other terms lead to phase matched frequencies which are different from those of $m = \pm 1$ and are removed by spectral filtering of the light, as shown in Fig. 1(c).) Our goal is to find conditions so that both the $m = 1$ and $m = -1$ terms support parametric down conversion simultaneously, with these two processes being the heart of our entangled photons source. The case using type-0 SPDC with $m = 0$ and type-II SPDC with $|m| = 1$ has been implemented experimentally [14].

The wave vector mismatch in Eq. (3) is given by

$$\Delta k_m(\omega_s, \omega_i) = k_Z(\omega_s) + k_Y(\omega_i) - k_Y(\omega_p) + \frac{2\pi m}{\Lambda} \quad (6)$$

for type II phase matching in a periodically poled crystal with poling period Λ ; the choice of Λ is set by our use of periodically-poled KTP with Y and Z representing directions of polarization in the crystal. The wave vectors are defined by $k_j(\omega) = \omega n_j(\omega)/c$, where $n_j(\omega)$ is the index of refraction for the polarization indexed by j , and c is the speed of light.

The two-photon joint spectral amplitudes $\beta(\omega_s, \omega_i)$ will be largest when ω_p is centered on angular frequency $\omega_p^{(m)} = \omega_s^{(m)} + \omega_i^{(m)}$ for which $\Delta k_m(\omega_s^{(m)}, \omega_i^{(m)}) = 0$. In order to achieve a polarization-entangled state, we select an operating point such that

$$\Delta k_1(\omega_s, \omega_i) = k_Z(\omega_s^{(1)}) + k_Y(\omega_i^{(1)}) - k_Y(\omega_p^{(1)}) + \frac{2\pi}{\Lambda} = 0$$

$$\Delta k_{-1}(\omega_i^{(1)}, \omega_s^{(1)}) = k_z(\omega_i^{(1)}) + k_y(\omega_s^{(1)}) - k_y(\omega_p^{(1)}) - \frac{2\pi}{\Lambda} = 0, \quad (7)$$

i.e., $\omega_s^{(1)} = \omega_i^{(-1)}$ and $\omega_s^{(-1)} = \omega_i^{(1)}$, which implies $\omega_p^{(1)} = \omega_p^{(-1)}$. The situation is illustrated in Fig. 2 for a case studied in the next section.

We develop a Taylor series about these points, introducing detuning frequencies $\xi_p = \omega_p - \omega_p^{(1)}$, $\xi_s = \omega_s - \omega_s^{(1)}$, and $\xi_i = \omega_i - \omega_i^{(1)}$. Expanding about these points

$$\begin{aligned} \Delta k_{\pm 1}(\omega_s, \omega_i) &= k_z(\omega_s) + k_y(\omega_i) - k_y(\omega_p) \pm \frac{2\pi}{\Lambda} \\ &\approx k_z(\omega_s^{(\pm 1)}) + k'_z(\omega_s^{(\pm 1)})\xi_s + k_y(\omega_i^{(\pm 1)}) + k'_y(\omega_i^{(\pm 1)})\xi_i \\ &\quad - k_y(\omega_p^{(\pm 1)}) - k'_y(\omega_p^{(\pm 1)})\xi_p \pm \frac{2\pi}{\Lambda}, \end{aligned} \quad (8)$$

hence

$$\Delta k_{\pm 1}^{(0)}(\xi_s, \xi_i) \approx k'_z(\omega_s^{(\pm 1)})\xi_s + k'_y(\omega_i^{(\pm 1)})\xi_i - k'_y(\omega_p^{(\pm 1)})(\xi_s + \xi_i) \quad (9)$$

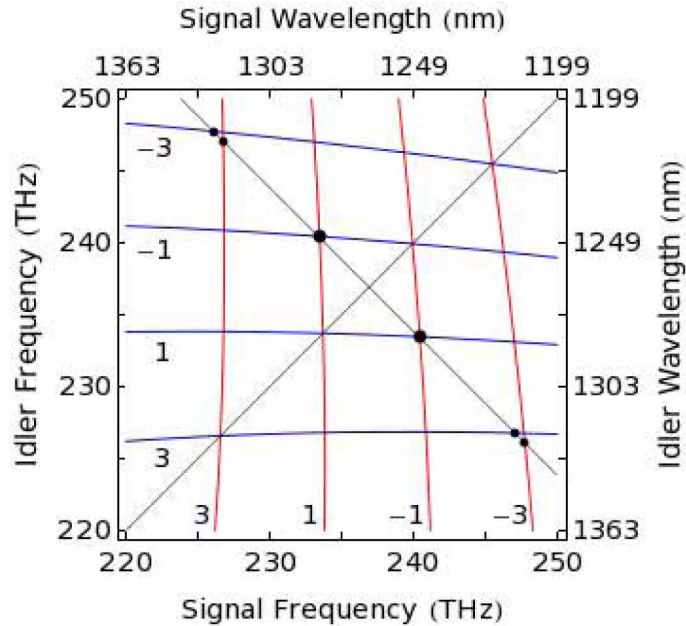


Fig. 2. Contours of $\Delta k_m(\omega_s, \omega_i) = 0$ (vertical, red) and $\Delta k_m(\omega_i, \omega_s) = 0$ (horizontal, blue) for $\Lambda = 1$ mm and $m = \pm 1, \pm 3$, as defined in Eq. (6). The axes are labeled by frequencies $\nu = \omega/2\pi$ as well as by the free space wavelengths $\lambda = c/\nu$. The line with negative slope obeys $\omega_s + \omega_i = \omega_p$ for $\lambda_p = 632.58$ nm. The line with positive slope indicates $\omega_s = \omega_i$. The large black dots represent the pairs $(\omega_s^{(1)}, \omega_i^{(1)}) = (\omega_i^{(-1)}, \omega_s^{(-1)})$ and $(\omega_i^{(-1)}, \omega_s^{(-1)}) = (\omega_s^{(-1)}, \omega_i^{(-1)})$ as defined in Eq. (7). The small black dots represent the pairs of daughter photons generated at the frequencies pairs $(\omega_s^{(\pm 3)}, \omega_i^{(\pm 3)})$ and $(\omega_i^{(\pm 3)}, \omega_s^{(\pm 3)})$. Additional frequency pairs will be generated for additional pairs of odd $\pm m$, but these are not in the range of the figure.

where the function $\Delta k_{\pm 1}^{(0)}(\xi_s, \xi_i) = \Delta k_{\pm 1}(\omega_s, \omega_i)$ and the primes denote differentiation with respect to the argument. In the special case $\omega_s^{(\pm 1)} = \omega_i^{(\mp 1)}$,

$$\Delta k_{-1}^{(0)}(\xi_i, \xi_s) \approx k'_z(\omega_i^{(1)}) \xi_i + k'_y(\omega_s^{(1)}) \xi_s - k'_y(\omega_p^{(1)}) (\xi_s + \xi_i) \quad (10)$$

where we have swapped the order of the arguments ξ_s and ξ_i as well as eliminating the variables $\omega_j^{(-1)}$ in favor of $\omega_j^{(1)}$.

Introducing the times

$$\begin{aligned} \tau_{1s} &= \left(k'_z(\omega_s^{(1)}) - k'_y(\omega_p^{(1)}) \right) \ell, \\ \tau_{1i} &= \left(k'_y(\omega_i^{(1)}) - k'_y(\omega_p^{(1)}) \right) \ell, \\ \tau_{-1s} &= \left(k'_y(\omega_s^{(1)}) - k'_y(\omega_p^{(1)}) \right) \ell, \text{ and} \\ \tau_{-1i} &= \left(k'_z(\omega_i^{(1)}) - k'_y(\omega_p^{(1)}) \right) \ell, \end{aligned} \quad (11)$$

we may write

$$\begin{aligned} \Delta k_1^{(0)}(\xi_s, \xi_i) \ell &\approx \tau_{1s} \xi_s + \tau_{1i} \xi_i \\ \Delta k_{-1}^{(0)}(\xi_i, \xi_s) \ell &\approx \tau_{-1s} \xi_s + \tau_{-1i} \xi_i. \end{aligned} \quad (12)$$

These times are the difference of the transit times for the pump and another mode across half of the crystal. This completes the formalism related to linearizing Eq. (3).

Fidelity of entanglement

We develop an analytic formula for the fidelity of an entangled state and follow up in the next section with numerical results for a particular Rb:KTP waveguide.

Interchanging the variables of integration $\omega_s \leftrightarrow \omega_i$ in Eq. (2) and then interchanging the order of integration, we may write

$$|\bar{2}\rangle = 2 \int d\omega_s d\omega_i \left[\beta(\omega_s, \omega_i) a_Y^\dagger(\omega_s) a_Z^\dagger(\omega_i) + \beta(\omega_i, \omega_s) a_Y^\dagger(\omega_i) a_Z^\dagger(\omega_s) \right] |0\rangle. \quad (13)$$

If we define two additional unnormalized two-photon states

$$|\bar{2}_\pm\rangle = \int d\omega_s d\omega_i \left[\beta(\omega_s, \omega_i) \pm \beta(\omega_i, \omega_s) \right] \left[a_Y^\dagger(\omega_s) a_Z^\dagger(\omega_i) \pm a_Y^\dagger(\omega_i) a_Z^\dagger(\omega_s) \right] |0\rangle, \quad (14)$$

we find these states are related by

$$|\bar{2}\rangle = \sum_{\pm} |\bar{2}_\pm\rangle \quad (15)$$

using $\sum_{\pm} 1 = 2$ and $\sum_{\pm} \pm 1 = 0$.

The normalized state from Eq. (2) is written

$$|2\rangle = \frac{|\bar{2}\rangle}{\langle \bar{2} | \bar{2} \rangle^{1/2}} \quad (16)$$

and, similarly, for Eq. (14), $|2_\pm\rangle = |\bar{2}_\pm\rangle / \langle \bar{2}_\pm | \bar{2}_\pm \rangle^{1/2}$. For an ideal polarization-entangled state, $|\bar{2}\rangle = |\bar{2}_\pm\rangle$ corresponding to $\beta(\omega_s, \omega_i) = \pm \beta(\omega_i, \omega_s)$. By considering the relevant matrix element of creation and destruction operators, the orthogonality relation $\langle \bar{2}_+ | \bar{2}_- \rangle = 0$ may be derived and so

$$\langle \bar{2} | \bar{2} \rangle = \sum_{\pm} \langle \bar{2}_\pm | \bar{2}_\pm \rangle. \quad (17)$$

The fidelity of a state is defined as $F = \text{Tr}\{\rho|2\rangle\langle 2|\}$ [15]. We will focus on to the case of the symmetric state by using the density matrix $\rho = |2_+\rangle\langle 2_+|$. (Any other choice of ρ leads to a lower figure for the fidelity assuming we are testing for the dominant state.) Substituting this form for ρ into the fidelity formula leads to

$$\begin{aligned} F &= |\langle 2_+|2\rangle|^2 \\ &= \frac{\langle \bar{2}_+|\bar{2}_+\rangle}{\langle \bar{2}|\bar{2}\rangle} \end{aligned} \quad (18)$$

using Eq. (16), Eq. (17), and $\langle \bar{2}_+|\bar{2}_-\rangle = 0$. The problem of finding the fidelity F has reduced to the evaluation of $\langle \bar{2}_\pm|\bar{2}_\pm\rangle$ because of Eq. (17).

We need the matrix element

$$\begin{aligned} &\langle 0|[a_Z(\bar{\omega}_i)a_Y(\bar{\omega}_s) \pm a_Z(\bar{\omega}_s)a_Y(\bar{\omega}_i)] [a_Y^\dagger(\omega_s)a_Z^\dagger(\omega_i) \pm a_Y^\dagger(\omega_i)a_Z^\dagger(\omega_s)]|0\rangle \\ &= 2\delta(\bar{\omega}_s - \omega_s)\delta(\bar{\omega}_i - \omega_i) \pm 2\delta(\bar{\omega}_s - \omega_i)\delta(\bar{\omega}_i - \omega_s) \end{aligned} \quad (19)$$

to write

$$\begin{aligned} \langle \bar{2}_\pm|\bar{2}_\pm\rangle &= \int d\bar{\omega}_s d\bar{\omega}_i d\omega_s d\omega_i [\beta(\bar{\omega}_s, \bar{\omega}_i) \pm \beta(\bar{\omega}_i, \bar{\omega}_s)]^* [\beta(\omega_s, \omega_i) \pm \beta(\omega_i, \omega_s)] \\ &\quad \times [2\delta(\bar{\omega}_s - \omega_s)\delta(\bar{\omega}_i - \omega_i) \pm 2\delta(\bar{\omega}_s - \omega_i)\delta(\bar{\omega}_i - \omega_s)]. \end{aligned} \quad (20)$$

As discussed in Appendix A, the foregoing discussion needs to be modified for a waveguide to take into account the differences in the spatial modes. Next, we define the direct integral

$$I = \int d\omega_s d\omega_i |\beta(\omega_s, \omega_i)|^2 \quad (21)$$

and the exchange integral

$$J = \int d\omega_s d\omega_i \beta^*(\omega_i, \omega_s)\beta(\omega_s, \omega_i). \quad (22)$$

In terms of the direct and exchange integrals,

$$\langle \bar{2}_\pm|\bar{2}_\pm\rangle = 8I \pm 8\text{Re}J. \quad (23)$$

The fidelity is given by

$$F = \frac{1}{2} \left(1 + \frac{\text{Re}J}{I} \right). \quad (24)$$

using Eq. (17), Eq. (18), and Eq. (26).

The integrals I and J are evaluated in Appendix C, leading to the expression

$$F = 1 - \frac{|\Delta\tau_+ - \Delta\tau_-|}{2(\Delta\tau_+ + \Delta\tau_-)} \quad (25)$$

using the symbols defined near Eq. (42). Eq. (25) implies $\frac{1}{2} \leq F \leq 1$. The maximum value $F = 1$ is achieved when $\Delta\tau_+ = \Delta\tau_-$. Restated, we obtain a high fidelity symmetric state when $|\tau_{1s} - \tau_{1i}| \approx |\tau_{-1s} - \tau_{-1i}|$, or equivalently, when $|k'_z(\omega_s^{(1)}) - k'_y(\omega_i^{(1)})| \approx |k'_y(\omega_s^{(1)}) - k'_z(\omega_i^{(1)})|$. In the limit of zero pump bandwidth (*i.e.*, a CW source), F is independent of both $k'_y(\omega_p^{(1)})$ and the crystal length $L = 2\ell$. While the natural range of F is 0 to 1, the assumption $c_1 = c_{-1}$ limits the range of F . Although we do not explore it here, $c_1 = -c_{-1}$, leads to $0 \leq F \leq \frac{1}{2}$ and is relevant for generating a pure state $|2_-\rangle$.

Table 1. Comparison of Present Sellmeier Equation to Experimental Results for Type I Second Harmonic Generation, which is the Inverse of Degenerate SPDC

	Λ (nm)	Expt. λ (nm)	Present λ (nm)
Katz <i>et al.</i> [21]	8.99	1064	1061
Samanta <i>et al.</i> [22]	9.01	1064	1062
Torabi-Goudarzi and Riis [23]	4	846	842

3. Fidelity of polarization-entangled states for our source

We propose and explore an operating point for our periodically-poled KTP (PPKTP) waveguide. We chose this medium for our waveguide because it has been used previously for SPDC-based sources in waveguides [14, 16, 17] and in the bulk [18, 19]. In our proposed system, shown in Fig. 1, a pump laser (possibly HeNe) is coupled to a waveguide formed from Rb diffused into a periodically-poled KTP crystal. Polarization-entangled signal and idler waves are generated through parametric down conversion. Upon exiting the crystal, the pump wavelength is removed from the beam. These waves pass through a bulk KTP crystal rotated by 90° for pulse timing compensation [5, 16, 20].

The index of refraction is usually parametrized using a Sellmeier equation. For KTP, we follow König and Wong [24] who recommend the Sellmeier equation of Fradkin *et al.* for $n_z^{(KTP)}$ [25] and who introduce a new Sellmeier equation for $n_y^{(KTP)}$. For the difference in the indices of KTP and RTP, $n_j^{(RTP)} - n_j^{(KTP)}$ for $j = Y, Z$, we use the measurements of Cheng *et al.* [26] who reports values for both crystals with one set of instruments. The index of refraction for the bulk crystals is given in Fig. 3. We followed this mixed procedure because the Sellmeier equation of König and Wong was developed specifically for PPKTP. This Sellmeier equation accounts for the reported type-0 phase matching for SHG in PPKTP as shown in Table 1.

We calculated the effective index of refraction for waveguides with Rb diffused into KTP (Rb:KTP) using the Sellmeier equations given above and the commercial software package Comsol Multiphysics including its RF (Radio Frequency) Module [27]. The waveguide parameters are the width w and the profile of the Rb dopants whose index profile decreases with depth into the crystal from the bulk RTP value to the bulk KTP value following the function $\text{erfc}(-Z/Z_0)$ [28] where the crystal surface is at $Z = 0$, and $Z \leq 0$ in the waveguide and in the crystal. We used a simulation region consisting of two quarter-circles filled with KTP with a $20 \mu\text{m}$ radius, a rectangular region of width w between the quarter circles to represent the waveguide proper, and a rectangular region of $(40 \mu\text{m} + w) \times 4 \mu\text{m}$ above to represent the air. A sketch of the simulation region is shown in Fig. 4 (top), along with the variation of the index of refraction in a particular case (bottom left). On the boundary, the fields were required to vanish. This approximation causes little error because the fields were exponentially confined. The simulation region was large enough that boundary effects were negligible as tested by comparing to a $30 \mu\text{m}$ radius boundary in selected cases and by visual inspection of the confined modes. The parameter w was chosen to ensure that the down converted photons are in a single mode for the signal and the idler.

In the standard approach, a crystal used for dispersion compensation matches the source crystal except for being half their length and rotated by 90° [5]. Here, to avoid the necessity of coupling into a second PPKTP waveguide, we propose using a rotated bulk KTP crystal instead. The compensation is adequate even though the materials are not exactly matched. For the case of a waveguide shown in Fig. 1, with a poling period $\Lambda=1 \text{ mm}$, $\lambda_s = 1247 \text{ nm}$ and $\lambda_i = 1284 \text{ nm}$.

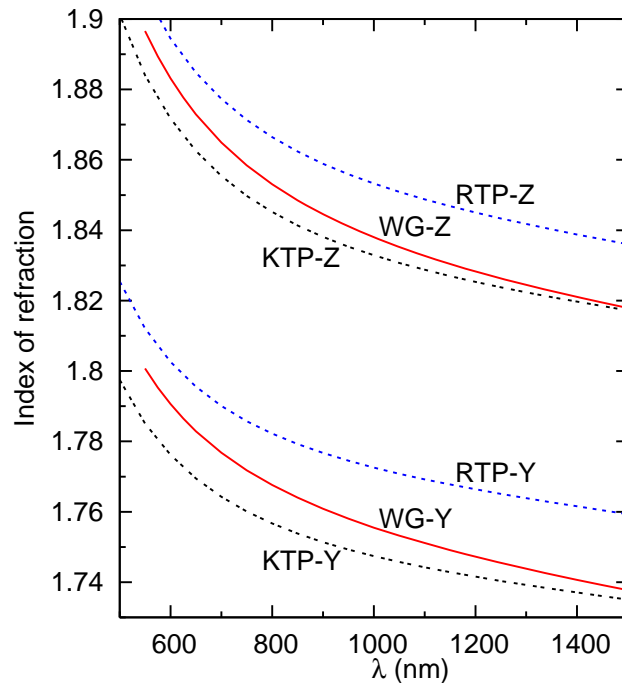


Fig. 3. The index of refraction for bulk RTP and KTP is given as a function of the free space wavelength for polarization along the crystal Y and Z axes. The effective index of refraction for the fundamental mode is given for an Rb:KTP waveguide (WG) with parameters $w = 3.5 \mu\text{m}$ and $Z_0 = 4.5 \mu\text{m}$.

The spread in the wave packet arises because photons converted near the exit face of the waveguide exit at almost the same time, whereas those converted near the entrance of the waveguide exit with a time difference given by $(L/c)[n_Z(\lambda_s) - n_Y(\lambda_s)]$ or $(L/c)[n_Z(\lambda_i) - n_Y(\lambda_i)]$, corresponding to $0.08069L/c$ and $0.08083L/c$. For the bulk crystal, the corresponding figures are $0.08325L/c$ and $0.08348L/c$. With a single length for the bulk crystal, we may compensate the average delay by choosing the bulk crystal length to be $0.9688/2$ of the waveguide instead of the traditional $1/2$. This deviates from the ideal compensation by $\pm 2 \times 10^{-5}L/c$, which is only $2.5 \times 10^{-4}L/c$ of the broadening by the waveguide. Hence, we conclude that bulk KTP may be used to compensate the timing of the broadening of two-photon wave packets in the KTP waveguides in analogy with the standard compensation scheme. For reference, if $L = 10 \text{ mm}$, then $L/c = 33 \text{ ps}$, the delay is about 2.6 ps , and the compensation error is about 0.7 fs .

We estimate that the conversion of photons from higher pump modes is negligible. Some of the higher pump modes will have odd parity under crystal $Y \leftrightarrow -Y$ about the waveguide centerline and hence yield a vanishing triple mode integral, yielding no signal and idler photons. The first higher mode with even parity, the third mode overall, yields a triple mode integral of 39 % that of the fundamental mode integral at $(\lambda_p, \lambda_s, \lambda_i) = (625, 1250, 1250) \text{ nm}$, and this factor enters the production rate squared, i.e., 0.15. Coupling to the input pump beam is likely to be weak compared to coupling to the fundamental pump mode of the waveguide. Finally, the effective index of refraction of this higher pump mode is 1.871 vs. 1.786 for the fundamental mode at $\lambda_p = 625 \text{ nm}$, suggesting the higher mode's signal and idler photons will be generated far from phase-matching conditions.

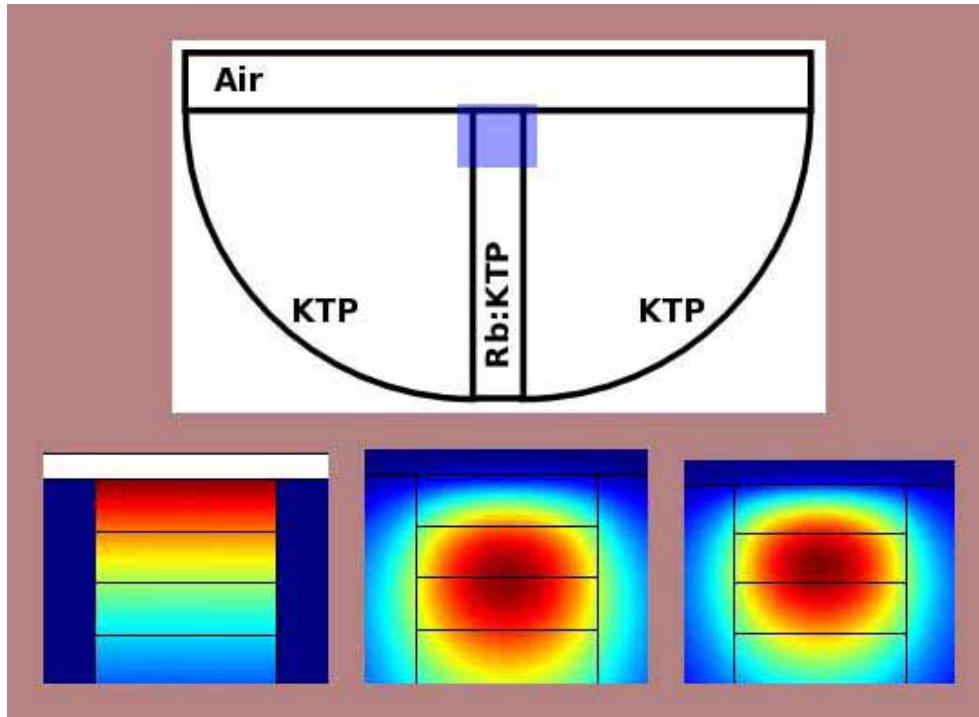


Fig. 4. (top) The simulation domain, including a $3.5 \mu\text{m}$ wide strip of Rb:KTP, two quarter circles of KTP of radius $20 \mu\text{m}$, and an air cap with a height of $4 \mu\text{m}$. The light blue region, a $4.5 \mu\text{m} \times 5.5 \mu\text{m}$ rectangle, is expanded in the panels below. (bottom left) The index of refraction, with white for air (1), blue for KTP (1.74), and the Rb:KTP strip ranging from the pure RTP value of 1.765 to 1.74. Specifically $n_Y(\lambda = 1265.4 \text{ nm})$ is shown. (bottom middle) The Z polarized mode at $\lambda = 1265.4 \text{ nm}$. (bottom right) The Y-polarized mode at $\lambda = 1265.4 \text{ nm}$. In the bottom three figures, horizontal lines are drawn at a depth of $1 \mu\text{m}$, $2 \mu\text{m}$, and $3 \mu\text{m}$. The inner vertical lines are $3.5 \mu\text{m}$ apart and mark the edge of the Rb-doped region.

When the wave vector mismatch given in Eq. (6) vanishes, the phase matching condition is satisfied. The poling period Λ required to achieve phase-matched degenerate SPDC in bulk KTP and a periodically poled waveguide of width $w = 3.5 \mu\text{m}$ and $Z_0 = 4.5 \mu\text{m}$ with the parameters defined in Table 2 is shown in Fig. 5. The poling periods required for type II phase matching are much longer than that needed for type 0 phase matching. This may be understood because the higher index of refraction for the Z polarized wave partially cancels the higher index of the (short wavelength) pump. Varying w or Z_0 has a very modest effect on the results as shown in Table 2. This Table also shows it is possible to obtain phase-matched degenerate SPDC with a HeNe laser $\lambda_p = 632.8 \text{ nm}$ for certain values of (w, Z_0) such as $(3.4, 4.5) \mu\text{m}$ and $(3.7, 4.5) \mu\text{m}$.

The signal, idler, and (doubled) pump wavelengths are shown in Fig. 6 as a function of the poling period Λ . To obtain Fig. 6 it was necessary to find the intersection points of curves $\Delta k(\omega_s, \omega_i) = -\Delta k(\omega_i, \omega_s)$, illustrated in Fig. 2 for the case of $\Lambda = 1 \text{ mm}$. Because we are imposing the constraints of Eq. (7), once the material, geometry, and Λ are chosen, there are no additional degrees of freedom. Hence, it is fortunate that the wavelengths are reasonably convenient, and that, with carefully chosen parameters, operation with HeNe laser for the pump should be possible. The curves are given for room temperature. The curves for the KTP are

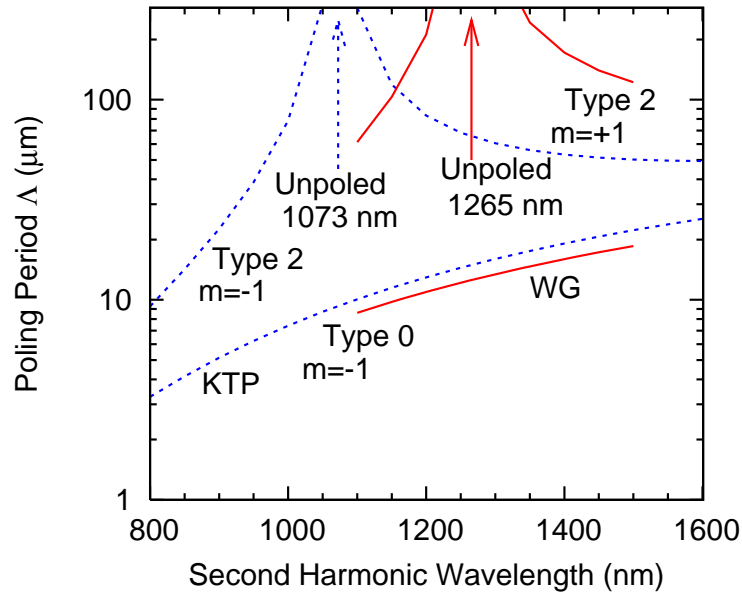


Fig. 5. Poling period as a function of degenerate SPDC wavelength ($\lambda_s = \lambda_i = 2\lambda_p$) for type-0 and type-II phase matching in both bulk KTP and in a Rb:KTP waveguide (WG) with parameters from Fig. 3. The wavelengths for unpoled type-II SHG are indicated. The curves for RTP are similar to KTP, but shifted to longer wavelengths including a shift of the unpoled wavelength to 1139 nm. The diffraction order m as defined in Eq. (6) is indicated on the graph; the type 0 phase matching always uses $m = -1$, but type II phase matching uses $m = -1$ for shorter wavelengths and $m = +1$ for longer wavelengths.

shifted upwards by about 0.6 nm for a 20 C rise above room temperature. Curves for RTP and the waveguide are similarly affected. The temperature coefficients for the index of refraction were taken from Emanuelli and Arie [29] for KTP and Mikami *et al.* for RTP [30].

Next, we come to the main goal of this paper, the estimate of the fidelity of the polarization-entangled states, according to Eq. (25). The results for KTP, RTP, and an Rb:KTP waveguide are shown in Fig. 7. (We have assumed colinear propagation, so the meaning of the results for the bulk crystals is hypothetical.) The main point is that high fidelities may be achieved for long poling periods. For example, for $\Lambda = 1$ mm, a fidelity of 0.987 may be achieved in the waveguide for $(\lambda_p, \lambda_s, \lambda_i) = (632.6, 1246.8, 1284.1)$ nm. As the poling period becomes increasingly long, the signal and idler wavelengths become more similar, as shown in Fig. 6.

The condition in Eq. (36) becomes increasingly important as $\Lambda \rightarrow \infty$, the small parameters $(|\tau_{\pm 1s} - \tau_{\pm 1i}| |\omega_s^{(1)} - \omega_i^{(1)}|)^{-1}$ growing from about 1 % at $\Lambda = 1$ mm to about 8 % at $\Lambda = 10$ mm. For the longer Λ and high precision studies, it would be necessary to consider the terms which were neglected in Eq. (35) and Eq. (40).

In an experiment, the fidelity may be affected by the spatial mode structure. These are very similar but not identical for the Y and Z polarized photons leaving the waveguide. For example, for 1250 nm photons, the overlap integral the electric fields for the two polarizations, (omitting the orthogonality due to polarization) is 0.97, when the two fields are normalized to unit self-overlap integrals. A simple way to nearly eliminate the effect of the spatial mode structure is to use a single mode optical fiber to produce identical spatial modes, albeit at the price of some coupling loss. (See Fig. 1.) Maintaining high efficiency throughout the optical path will

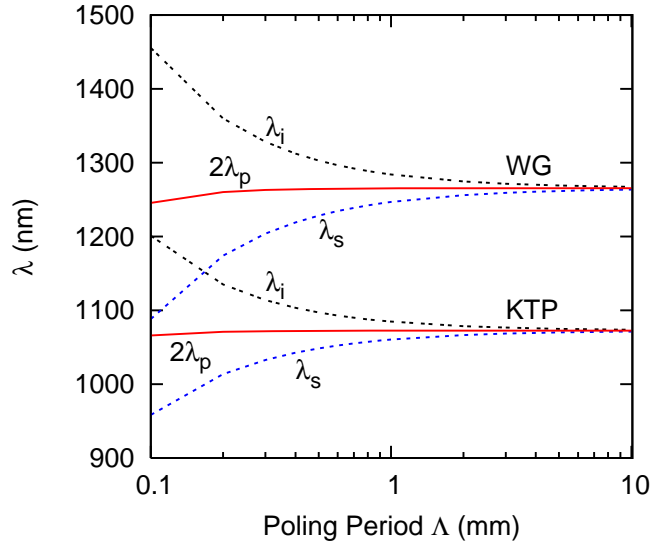


Fig. 6. The signal, idler, and pump wavelengths (with polarizations along the crystal axes Z , Y , and Y , respectively) as a function of the poling period for bulk KTP and for a waveguide (WG) using the parameters from Fig. 3. The curves for bulk RTP are between the two families shown here. The values for $\lim \Lambda \rightarrow \infty$ are reported in Table 2.

require considerable care, including the use of antireflective coatings which reduces the need for reliance in post selection by reducing the fraction of broken pairs. We also note that these losses do not affect fidelity, unless the contributions of background light or detector dark count rates become significant. In a similar way, polarization and frequency-dependent absorption can ameliorate the effect of an imbalance (i.e., deviation from unity) in the c_1/c_{-1} ratio discussed in Appendix B.

4. Concluding remarks

We have presented a proposal for a source of intrinsically-created polarization-entangled photons using type II parametric down conversion in a periodically-poled Rb:KTP waveguide. The

Table 2. Pump and Degenerate SPDC Wavelengths (nm) in Unpoled Rb:KTP Waveguides and Bulk RTP and KTP^a

w (μm)	Z_0 (μm)	λ_p (nm)	$\lambda_s = \lambda_i$ (nm)
3.0	4.5	634.9	1269.9
3.5	4.5	632.7	1265.4
4.0	4.5	634.3	1268.5
3.5	6.0	629.8	1259.6
bulk RTP		569.5	1139.0
bulk KTP		536.3	1072.6

^aThe parameters of width w and depth Z_0 are defined in the text. By interpolation, the HeNe wavelength of 632.8 nm may be applied to a waveguide with $w = 3.4 \mu\text{m}$ or $w = 3.7 \mu\text{m}$ and $Z_0 = 4.5 \mu\text{m}$.

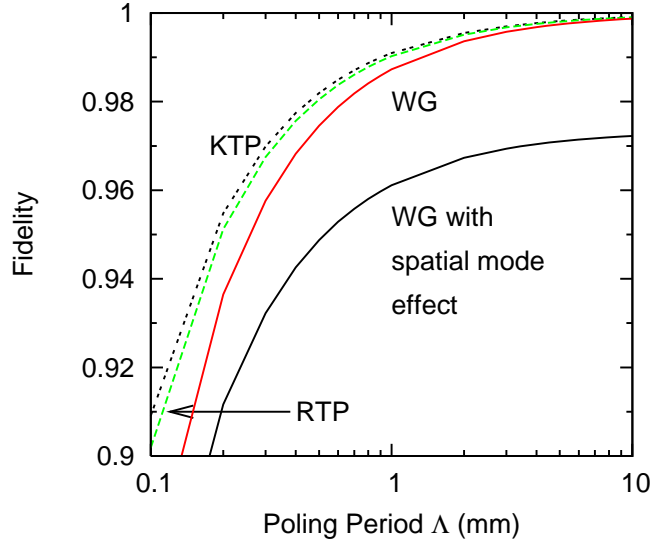


Fig. 7. The fidelity, according to Eq. (25) for bulk KTP, bulk RTP, and the Rb:KTP waveguide (WG) using the parameters from Fig. 3. (A single mode is assumed for bulk KTP and bulk RTP which give these a model character.) The spatial mode effect is estimated to reduce the fidelity by a factor of 0.97 for $\Lambda \geq 0.2$ mm, falling to 0.89 for $\Lambda = 0.1$ mm. However, the spatial mode effect can be largely eliminated, as discussed in the text.

new source's simple optical design is expected to be more stable and easier to implement than previously demonstrated sources. The brightness and fidelity are expected to be comparable to the best existing sources.

The key feature of the new source is the simultaneous quasi-phase matching of photons using both orders $m = \pm 1$ of the periodically poled KTP waveguide. A disadvantage of the scheme is that the available pump, signal, and idler wavelengths are highly constrained. However, we have shown that solutions are possible and even a common HeNe laser generating light at 632.8 nm may be used as a pump for certain geometries.

A. Spatial mode effect

After the introduction of Eq. (1), we noted that the effect of spatial modes disappears if the modes are identical. Here, we consider explicitly the effect of different spatial modes. In an ideally entangled Bell state of the type $|YZ\rangle + |ZY\rangle$, we may perform the interchange $Z \leftrightarrow Y$ with the state remaining invariant [31, 32]. (Other authors use $|HV\rangle + |VH\rangle$ for our state $|YZ\rangle + |ZY\rangle$.)

To avoid too much notational complexity, we will take $\beta(\omega_s, \omega_i) \approx \beta(\omega_i, \omega_s)$ in this Appendix. In analogy with Eq. (20), the norm is

$$\begin{aligned}
 \langle \bar{2}_{\pm} | \bar{2}_{\pm} \rangle &= 2 \int d\bar{\omega}_s d\bar{\omega}_i d\omega_s d\omega_i d\bar{r}_s d\bar{r}_i \beta^*(\bar{\omega}_s, \bar{\omega}_i) \beta(\omega_s, \omega_i) \\
 &\quad \sum_{\pm} [U_Y^*(\bar{r}_s, \bar{\omega}_s) U_Z^*(\bar{r}_i, \bar{\omega}_i) \pm U_Y^*(\bar{r}_i, \omega_i) U_Z^*(\bar{r}_s, \bar{\omega}_s)] [U_Y(\bar{r}_s, \omega_s) U_Z(\bar{r}_i, \omega_i) \pm U_Y(\bar{r}_i, \omega_i) U_Z(\bar{r}_s, \omega_s)] \\
 &\quad [2\delta(\bar{\omega}_s - \omega_s) \delta(\bar{\omega}_i - \omega_i) \delta(\bar{r}_s - \bar{r}_i) \delta(\bar{r}_i - \bar{r}_i) \pm 2\delta(\bar{\omega}_s - \omega_i) \delta(\bar{\omega}_i - \omega_s) \delta(\bar{r}_s - \bar{r}_i) \delta(\bar{r}_i - \bar{r}_s)] \\
 &= 8I \pm 8J \int d\bar{r}_s d\bar{r}_i U_Y^*(\bar{r}_s, \omega_s) U_Z^*(\bar{r}_i, \omega_i) U_Y(\bar{r}_i, \omega_i) U_Z(\bar{r}_s, \omega_s) \\
 (26)
 \end{aligned}$$

using the normalization integral $\int d\vec{r} |U_j(\vec{r}_s, \omega_s)|^2 = 1$ for $j = Y, Z$. If we assume that the exchange integral is independent of frequency, then we have

$$\langle \bar{2}_\pm | \bar{2}_\pm \rangle = 8I \pm 8J \left| \int d\vec{r} U_Y(\vec{r})^* U_Z(\vec{r}) \right|^2. \quad (27)$$

Thus, the net effect of the spatial mode structure on the fidelity is to make the exchange integral smaller by a factor of the spatial mode overlap integral in Eq. (24). For our waveguide, for $\lambda = 625$ nm, the spatial mode integral factor reduces the fidelity by a factor of 0.9738. The spatial modes are show for this case in Fig. 4 (bottom middle and bottom right). The modes are seen to be very similar, although not identical. The factor is only a weak function of the wave vector mismatch. For example, for $\Lambda = 0.1$ mm, 0.5 mm, and 1 mm, we obtain values of 0.8906, 0.9693, and 0.9697.

As discussed in Sec. III, near $\Lambda = 1$ mm, the fidelity (omitting the spatial mode effect) can exceed 0.98. Hence, this may be the limiting factor in obtaining high fidelity. Manipulating the signal and idler beams after waveguide may be used to relieve this problem, in analogy to the temporal compensators which were established in the 1990's. The simplest approach is to let the spatial modes enter a single mode fiber without polarization dependence.

B. Generation rates of two output channels

The coefficients c_1 and c_{-1} are proportional to matrix elements of the interaction Hamiltonian for parametric down conversion. This theory was developed for periodically poled waveguides by Fiorentino and coworkers [17] adapting an earlier development for parametric down conversion in periodically poled bulk crystals [11]. Indeed, the development of the present paper is anticipated to a certain extent by Ref. [11] in that they expand the position-dependent nonlinear coefficient $d(x, z)$ as a Fourier series

$$d(x, z) = \sum_{n=-\infty}^{+\infty} d_n(x) e^{-inKz} \quad (28)$$

which is Eq. (8) of Ref. [11]. (Our co-ordinate system is explained in Fig. 1(a).) They remark "the only term in Eq. (8) which will lead to a constructive interaction between the pump wave and the signal and idler is $d_n(x)$." They then present a phase matching equation equivalent to our Eq. (6). Here, we consider more than one such term. Each yields the same form for the interaction matrix element which is given in Eq. (11) of Ref. [17] which is

$$\langle f | H_I | i \rangle = \frac{d\hbar(2\mathcal{P}_p \omega_s \omega_i)^{1/2}}{(\epsilon_0 c n_s^2 n_i^2 n_p)^{1/2}} L \text{sinc}\left(\frac{\Delta k L}{2}\right) \int_A dx dy U_p(x, y) U_i^*(x, y) U_s^*(x, y) \quad (29)$$

as written in the notation of the reference. Here, d is the effective nonlinear coefficient $(2/\pi)d_{bulk}$ [11], \mathcal{P}_p is the pump power, ϵ_0 is the electric constant, c is the speed of light, the n are indices of refraction, L is the crystal length, and A is the cross-sectional area of the waveguide, and the various U are the modes in the waveguide. In our case, we must remember that the n and d refer to the applicable polarization. We may write the ratio

$$\frac{c_{-1}}{c_1} = \frac{d_{YZ}(\omega_p, \omega_s, \omega_i)}{d_{YZ}(\omega_p, \omega_i, \omega_s)} \frac{n_Z(\omega_i)}{n_Z(\omega_s)} \frac{n_Y(\omega_s)}{n_Y(\omega_i)} \frac{G(\omega_p, \omega_s, \omega_i)}{G(\omega_p, \omega_i, \omega_s)} \quad (30)$$

with

$$G(\omega_p, \omega_s, \omega_i) = \int_A dx dy U_Y(x, y; \omega_p) U_Z^*(x, y; \omega_s) U_Y^*(x, y; \omega_i) \quad (31)$$

where (ω_s, ω_i) is evaluated at $(\omega_s^{(1)}, \omega_i^{(1)})$.

We estimate the dispersion of the nonlinear coefficients using Miller's rule [33], namely

$$d_{YZY}(\omega_p, \omega_s, \omega_i) \approx \delta_{YZY} \chi_{YY}(\omega_p) \chi_{ZZ}(\omega_s) \chi_{ZZ}(\omega_i) \quad (32)$$

where δ_{YZY} is taken to be a constant and the χ are the linear susceptibilities, which are related to the index of refraction by $4\pi\chi_{jj}(\omega) = n_j^2(\omega) - 1$. This permits us to estimate

$$\frac{c_{-1}}{c_1} = \frac{n_Z^2(\omega_s) - 1}{n_Z^2(\omega_i) - 1} \frac{n_Y^2(\omega_i) - 1}{n_Y^2(\omega_s) - 1} \frac{n_Z(\omega_i)}{n_Z(\omega_s)} \frac{n_Y(\omega_s)}{n_Y(\omega_i)} \frac{G(\omega_p, \omega_s, \omega_i)}{G(\omega_p, \omega_i, \omega_s)}. \quad (33)$$

In the limit of degenerate parametric down conversion, *i.e.*, inverse second harmonic generation, $\omega_s = \omega_i$, so $c_{-1}/c_1 = 1$. This limit is obtained as $\Lambda \rightarrow \infty$. As may be seen from the derivation in the text and Appendix C, the fidelity must be reduced by a factor of $2[(c_{-1}/c_1) + (c_1/c_{-1})]^{-1} \leq 1$ assuming $I_{++} \approx I_{--}$ using the symbols defined in Eq. (35).

Numerical calculations for $\Lambda = 0.1$ mm, 0.5 mm, and 1 mm show that c_{-1}/c_1 is 1.2084, 1.0365, and 1.0125 for the three cases, respectively. The deviation from unity is almost entirely due to the triple mode integral. The factors involving the index of refraction in Eq. (33) differ from unity by less than 10^{-4} for $\Lambda \geq 0.1$ mm. Using the expression at the end of the previous paragraph, the fidelity needs to be reduced from that shown in Fig. 7 by a factor of 0.9823, 0.9994, and 0.9999, all of which are smaller than deviations from unity shown in the plot for the associated value of Λ . Hence, the approximation $c_1 \approx c_{-1}$ is justified.

C. Evaluation of direct and exchange integrals

The direct integral is given in Eq. (21) and the form of β is given by Eq. (3).

$$I = \int d\omega_s d\omega_i [\alpha(\omega_s + \omega_i)]^2 \left\{ \sum_{\pm} \text{sinc}[\Delta k_{\pm 1}(\omega_s, \omega_i)\ell] \right\}^2. \quad (34)$$

In an obvious notation, let

$$I = I_{++} + I_{--} + I_{+-} + I_{-+}. \quad (35)$$

There are large contributions where $\omega_s \approx \omega_s^{(1)}$ and $\omega_i \approx \omega_i^{(1)}$ to I_{++} , and large contributions when $\omega_s \approx \omega_i^{(1)}$ and $\omega_i \approx \omega_s^{(1)}$ to I_{--} , but the mixed terms are nowhere large, assuming that $(\omega_s^{(1)}, \omega_i^{(1)})$ is always far from $(\omega_i^{(1)}, \omega_s^{(1)})$ on the scale of oscillations of the sinc function. Formally, we require

$$1 \ll |\tau_{\pm 1s} - \tau_{\pm 1i}| |\omega_s^{(1)} - \omega_i^{(1)}| \quad (36)$$

to neglect $I_{+-} = I_{-+}$. Equation (??) may be achieved in practice with periodically poled KTP.

We may write I_{++} as an integral over ξ_s and ξ_i as

$$\begin{aligned} I_{++} &= \int d\xi_s d\xi_i [\alpha^{(0)}(\xi_s + \xi_i)]^2 \text{sinc}^2 [\Delta k_1^{(0)}(\xi_s, \xi_i)\ell] \\ &\approx \int d\xi_s d\xi_i [\alpha^{(0)}(\xi_s + \xi_i)]^2 \text{sinc}^2 (\tau_{1s}\xi_s + \tau_{1i}\xi_i). \end{aligned} \quad (37)$$

For I_{--} , we interchange ω_s and ω_i ,

$$I_{--} = \int d\xi_i d\xi_s [\alpha^{(0)}(\xi_i + \xi_s)]^2 \text{sinc}^2 [\Delta k_{-1}^{(0)}(\xi_i, \xi_s)\ell]$$

$$\approx \int d\xi_s d\xi_i \left[\alpha^{(0)}(\xi_s + \xi_i) \right]^2 \text{sinc}^2(\tau_{-1s}\xi_s + \tau_{-1i}\xi_i). \quad (38)$$

The exchange integral is given by

$$J = \int d\omega_s d\omega_i [\alpha(\omega_s + \omega_i)]^2 \sum_{\pm} \{ \text{sinc}[\Delta k_{\pm 1}(\omega_s, \omega_i)\ell] \text{sinc}[\Delta k_{\pm 1}(\omega_i, \omega_s)\ell] + \text{sinc}[\Delta k_{\pm 1}(\omega_s, \omega_i)\ell] \text{sinc}[\Delta k_{\mp 1}(\omega_i, \omega_s)\ell] \}. \quad (39)$$

In a similar obvious notation similar to that above, let

$$J = J_{++} + J_{--} + J_{+-} + J_{-+}. \quad (40)$$

In this case, the terms J_{++} and J_{--} may be neglected because the arguments to the two sinc functions are never simultaneously small. However, for $J_{+-} = J_{-+}$ both arguments may be simultaneously small.

$$\begin{aligned} J_{+-} &= \int d\xi_s d\xi_i \left[\alpha^{(0)}(\xi_s + \xi_i) \right]^2 \text{sinc}[\Delta k_1^{(0)}(\xi_s, \xi_i)\ell] \text{sinc}[\Delta k_{-1}^{(0)}(\xi_i, \xi_s)\ell] \\ &\approx \int d\xi_s d\xi_i \left[\alpha^{(0)}(\xi_s + \xi_i) \right]^2 \text{sinc}(\tau_{1s}\xi_s + \tau_{1i}\xi_i) \text{sinc}(\tau_{-1s}\xi_s + \tau_{-1i}\xi_i). \end{aligned} \quad (41)$$

If we take the pump bandwidth to be zero, Eq. (5) applies. Introducing $\delta\tau_{\pm} = \tau_{\pm 1s} - \tau_{\pm 1i}$, the integrals in Eq. (37) and Eq. (38) reduce to

$$\begin{aligned} I_{\pm\pm} &= \int d\xi \text{sinc}^2(\delta\tau_{\pm}\xi) \\ &= \frac{\pi}{\Delta\tau_{\pm}}, \end{aligned} \quad (42)$$

where $\Delta\tau_{\pm} = |\delta\tau_{\pm}|$. To obtain Eq. (42), we use the change of variables $\xi_p = \xi_s + \xi_i$ and $\xi = (\xi_s - \xi_i)/2$ which has a unit Jacobian; also $\xi_s = -\xi_i$ where the δ function of Eq. (5) is non-zero. Similarly, from Eq. (41),

$$\begin{aligned} J_{+-} &= \int d\xi \text{sinc}(\delta\tau_+\xi) \text{sinc}(\delta\tau_-\xi) \\ &= \pi \frac{\Delta\tau_+ + \Delta\tau_- - |\Delta\tau_+ - \Delta\tau_-|}{2\Delta\tau_+\Delta\tau_-}. \end{aligned} \quad (43)$$

We may use $\Delta\tau_{\pm}$ instead of $\delta\tau_{\pm}$ because the sinc function is even.

We may write

$$I \approx \sum_{\pm} I_{\pm\pm} = \pi \frac{\Delta\tau_+ + \Delta\tau_-}{\Delta\tau_+\Delta\tau_-} \quad (44)$$

and $J \approx 2J_{+-}$. These expressions for I and J , combined with Eq. (24), lead to Eq. (25).

Acknowledgments

Conversations with Eite Tiesinga are gratefully acknowledged. This work was supported in part by the Intelligence Advanced Research Projects Activity (IARPA) entangled photon source program.